Proceedings of the 21st ICSMGE, Vienna, Austria, 14 – 19 June 2026. Pistrol, Adam & Schweiger (eds.)
Published by: ÖGG, Austrian Society for Geomechanics, Salzburg, Austria, ISBN 978-3-9503898-4-5
https://doi.org/10.53243/ICSMGE2026-1297

Assessment of the regional subsidence in Mexico City using a geostatistical model

Maria Madrigal, Eduardo Botero
Instituto de Ingeniería, Universidad Nacional Autónoma de México (UNAM), Mexico, EBoteroJ@iingen.unam.mx

Carlos Díaz
Instituto de Investigaciones en Matemáticas Aplicadas y en Sistemas, Universidad Nacional Autónoma de México (UNAM), Mexico

ABSTRACT: The overexploitation of the groundwater resources underlying the lacustrine deposits of Mexico City has triggered regional subsidence that manifests itself through the sinking of the ground surface, damaging infrastructure and public services. In this work, R, a free software environment for statistical computing tools, was used to analyze and assess the evolution of this phenomenon in the city, by considering space–time data from surface benchmarks located in the lacustrine zone. The database is composed of 206 spatial features and 12 time points, for a total of 24 years of monitoring between 1983 and 2007. Results show that the *separable* variogram model was the one that best represented the spatial and temporal correlation of the phenomenon in the area of study. The validation process consisted of comparing direct measurements made in 2016 and 2021 with those obtained from the model for the same years. For the year 2030, the maximum cumulative subsidence value was 13 m, and the highest mean rate was 25.06 cm/year near the Mexico City International Airport.

KEYWORDS: Regional subsidence, kriging, geostatistics, space-time models, R.

1 INTRODUCTION

The Valley of Mexico is one of the four valleys that make up the Basin of Mexico (Ossa et al. 2019). The subsoil of the Valley of Mexico is divided into three geotechnical zones: (1) the Hill zone (Zone I) is mainly composed of a surface layer of lava flows or volcanic tuffs (Shapiro et al. 2001, Arroyo et al. 2013); (2) the Transition zone (Zone II) presents alluvial sandy and silty layers interbedded with occasional clay layers (Shapiro et al. 2001, Arroyo et al. 2013); and (3) the Lake zone (Zone III) consists of a 30 to 100 m thick deposit of clay, underlain by sands (Shapiro et al., 2001). Mexico City is in the southern section of the Basin of Mexico, and most of the city is settled in the Lake zone.

At a depth of approximately 50 m of the soil profile of the lacustrine area of Mexico City, an upper granular aquifer is made up of Quaternary alluvial deposits, volcaniclastic and pyroclastic rocks, and Plio-Quaternary basaltic-andesitic rocks are found (Hernández-Espriu et al. 2014). The exploitation of this aquifer began in the mid-19th century to supply water to the city's population; however, the intense extraction of water from wells in response to population growth has triggered a regional consolidation of lacustrine deposits. This phenomenon is manifested by the lowering of the land surface as voids in the soil are reduced and forces between soil particles increase. Currently, Mexico City and its metropolitan area are heavily populated with ~22 million inhabitants (INEGI, 2020). For practical purposes, the aquifer underlying the clay deposits provides drinking water for most of this population (Hernández-Espriu et al., 2014).

The importance of analyzing the regional subsidence in the lacustrine zone of Mexico City lies in the fact that the accumulation of settlements can affect the functionality and safety of the drainage system, gas stations, underground storage tanks, oil pipelines and infrastructure (Hernández- Espriu et al. 2014). In the last 100 years, this phenomenon has led to having cumulative ground subsidence of more than 8 m in some areas of the lacustrine zone of the Valley of Mexico compared to a reference point outside the lake zone (Ovando et al. 2003, 2013; Arroyo et al. 2013). In addition, this phenomenon modifies the soil properties that determine the dynamic behavior of the material during a seismic event. Hence, some studies focused on measuring the ground subsidence for several sites in Mexico City, while others were developed to analyze the effects of this phenomenon on the static and dynamic properties of lacustrine deposits and their seismic response during a seismic event.

The modeling of dynamic processes evolving in both space and time is critical in many scientific and engineering fields, because a probabilistic framework for data analysis and predictions is provided considering the spatial-time dependence of the observations (Kyriakidis & Journel 1999). For this reason, and because there is not an specific theoretical or empirical method to analyze the subsidence phenomenon in the lacustrine zone of Mexico City, the purpose of this work is to assess the behavior in space and time of the surface benchmarks located in the Lake zone of Mexico City and to analyze the evolution of the regional subsidence phenomenon from a statistical point of view using a space–time model.

2 SPACE-TIME DATA ANALYSIS METHODS

Geostatistics is a set of statistical techniques used for the analysis of stochastic processes whose domain $\mathcal{D}$ is continuous in a subset of $\mathbb{R}^d$. If we denote the random variable of interest by Z and s as an arbitrary point in $\mathcal{D}$ then the stochastic process of interest is denoted as $\{Z(s): s \in \mathcal{D}\}$, and represents the set of possible observations of $Z(s)$, which form a random field (Cressie, 1993). One of the usual tasks in geostatistical data analysis is the prediction of Z at unvisited locations s_0. In general, geostatistical analysis consists of the following four stages: exploration analysis, structural analysis, spatial modeling, and prediction using Krige.

In the spacetime package of the R statistical program (R Core Team, 1993; RStudio Team, 2015), four grid formats for spatiotemporal data are included, but in this work, a spacio-temporal full drataframe (STFDF) is used, which means that every spatial feature will have a time observation point completing a perfectly filled rectangle with zero missing values (Figure 1).

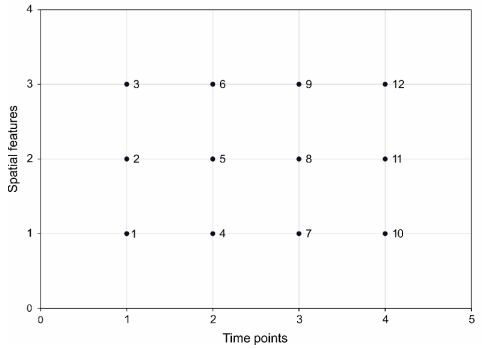

Figure 1. Full grid layout (modified from Pebesma, 2012).

To perform estimations and predictions of the variable *Z* at unobserved locations, the random field *Z* is commonly assumed to be stationary and spatially isotropic, so that it can be characterized through the mean μ and a covariance function C_{st}. Under this assumption, the space-time covariance depends only on the separating distances across space $h \in \mathbb{R}^2 \geq 0$ and time $u \in \mathbb{R}^+$, this is, $C(h,u) = Cov\big(Z(s,t), Z(\tilde{s},\tilde{t})\big)$, where $h = \|s - \tilde{s}\|$ and $u = \|t - \tilde{t}\|$ are the spatial and temporal distances of a pair of points (s,t), $(\tilde{s},\tilde{t}) \epsilon\, S \times T$. The spatio-temporal variograms $\gamma_{st}(h,u) = C_{st}(0,0) - C_{st}(s,t)$ are often used to characterize a phenomenon *Z*, since unlike the covariance, it is not necessary to estimate the mean of *Z* to compute $\gamma_{st}(h,u)$ (Gräler et al. 2016). The variogram models implemented in the R *gstat* package make it possible to relate objects to spatiotemporal characteristics and to estimate these in space and time.

A variogram is a critical input to geostatistical studies. It is a tool used to investigate and quantify the spatial variability of the phenomenon under study, and also it is required in most geostatistical estimation or simulation algorithms to reproduce the process (Gringarten and Deutsch, 2001).

The *separable* variogram model of Equation (1) has a significant computational advantage when each spatial object has an observation at each temporal instance, i.e., when the data are organized in a complete grid layout as shown in Figure 1 (Pebesma, 2012). On the other hand, it has the simplest form for spatio-temporal models, where the dependence on the spatial coordinates is separated from the dependence on the temporal coordinates (De Iaco et al. 2011).

$$\gamma_{sep}(h,u) = \text{sill} \cdot \big(\bar{\gamma}_s(h) + \bar{\gamma}_t(u) - \bar{\gamma}_s(h)\,\bar{\gamma}_t(u)\big) \qquad (1)$$

where, the sill is the value at which the variogram reaches a plateau and it represents de maximum variability between a pair of data points. Beyond this distance, the points are no longer correlated. h and u are the spatial and temporal distances of a pair of points, and $\bar{\gamma}_s$ and $\bar{\gamma}_t$ are the standardized spatial and temporal variogram (Gräler et al. 2016).

This model extends to the *product-sum* variogram model (Equation (2)) developed by De Cesare et al. (2001) and De Iaco et al. (2001), where, unlike the previous one, they considered non-separable variograms to represent the spatiotemporal variability of the data.

$$\begin{aligned}\gamma_{ps}(h,u) = {} & (k \cdot \text{sill}_\text{t} + 1)\gamma_s(h) \\ & + (k \cdot \text{sill}_\text{s} + 1)\gamma_t(u) \\ & - k\gamma_s(h)\gamma_t(u)\end{aligned} \qquad (2)$$

Here, $\gamma_s(h)$ and $\gamma_t(u)$ are the spatial and temporal variograms respectively, and *k* is a positive parameter that defines the joint sill, sill_st, in terms of the spatial sill_s and temporal sill_t (Equation (3).

$$\text{sill}_\text{st} = k \cdot \text{sill}_\text{s} \cdot \text{sill}_\text{t} + \text{sill}_\text{s} + \text{sill}_\text{t}. \qquad (3)$$

Bilonick (1988) proposed the *sum-metric* model (Equation (4)), an extension of the separable variogram model, using zonal and geometric anisotropy to resolve the differences between spatial and temporal variability (Snepvangers et al. 2003).

$$\begin{aligned}\gamma_{sm}(h,u) = {} & \gamma_s(h) + \gamma_t(u) \\ & + \gamma_{joint}\left(\sqrt{h^2 + (k \cdot u)^2}\right)\end{aligned} \qquad (4)$$

where, γ_{joint} is the joint variogram and *k* is the anisotropy.

The *separable*, *product-sum*, and *sum-metric* differ mostly in how they compute the dependence between the spatial and temporal objects of the data. The *separable* model has the lowest flexibility which implies that spatial correlation structure is the same for all time lags and the temporal correlation structure is the same for all spatial lags. On the other hand, the *product-sum* model has the most flexible of these three models since it allows to input a space-time direction of correlation (anisotropy). However, this flexibility implies higher computational complexity due to the estimation of more parameters.

3 SPACE-TEMPORAL ANALYSIS OF THE REGIONAL SUBSIDENCE IN MEXICO CITY

3.1 *Description of the database*

The General Directorate of Hydraulic Construction and Operation (DGCOH) of the Federal District government, today Mexico City Water Bureau (SACMEX, in Spanish), began in 1976 with the installation of surface benchmarks to understand the evolution of subsidence and to provide solutions to the problems of hydraulic systems in the Valley of Mexico (SIMOH, 2015).

The monitoring system consists of 1931 surface benchmarks distributed in the Hill zone (Zone I), the Transition zone (Zone II), and the Lake zone (Zone III), leveled during 1983–2016 with a reading every two years, approximately. However, it is essential to mention that these data have missing ground elevation records.

To perform the statistical analysis and develop a spatial–temporal model, the information provided was reviewed and the database was built considering the measurements of the following superficial references: (1) benchmarks located in the Lake zone because it is where the regional subsidence phenomenon manifests itself, and (2) also those that have 1983 as the initial year of monitoring and presented at most two missing records in non-consecutive years. These missing readings were obtained from a linear interpolation considering the trend of measurements. This process was performed to have a whole space–time grid layout (STF) of observations (Figure 1), where each spatial point s_i, i = 1, …, n, has a measurement in each one of the monitoring years t_j, j = 1, …, m.

At the end of this data review, 206 spatial features remained, each with fourteen time points (1983, 1985, 1987, 1989, 1992, 1994, 1996, 1998, 2000, 2002, 2005, 2007, 2016, 2021) for a total of 38 years of monitoring. It should be noted that the time points of the years 2016 and 2021 were not considered in the space–time analysis, since they were used to validate the ground elevations determined with the geostatistical model.

The mean rate of subsidence in centimeters per year (cm/year) was determined for each benchmark and the Jenks Natural Breaks classification method (Jenks & Caspall, 1971) was used to organize them into six classes:(1) 1.1–5.9 cm/year, (2) 5.9–11.1 cm/year, (3) 11.1–16.7 cm/year, (4) 16.7–23.1 cm/year, (5) 23.1–28.8 cm/year and (4) 28.8–35.1 cm/year (Figure 2). This classification is a data-clustering method used

to estimate the best arrangement of values into different categories when it does not exist a standard or specific categories classification. Here the variance within classes is minimized and it is maximized between them. Also, it is important to underline that these classes are specific to this dataset of subsidence values therefore it is not recommended to be used in another dataset.

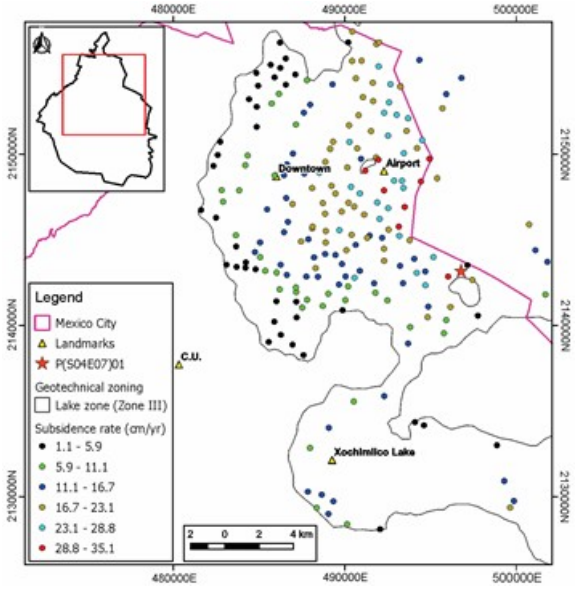

Figure 2. Subsidence rate of each superficial benchmark during 1983-2007.

Between 1983 and 2007, the lowest and highest mean rates were 1.1 and 35.1 cm/year, respectively. In the benchmark P(S04E07)01, where the highest subsidence rate was recorded, 8.41 m cumulative subsidence occurred (Figure 2).

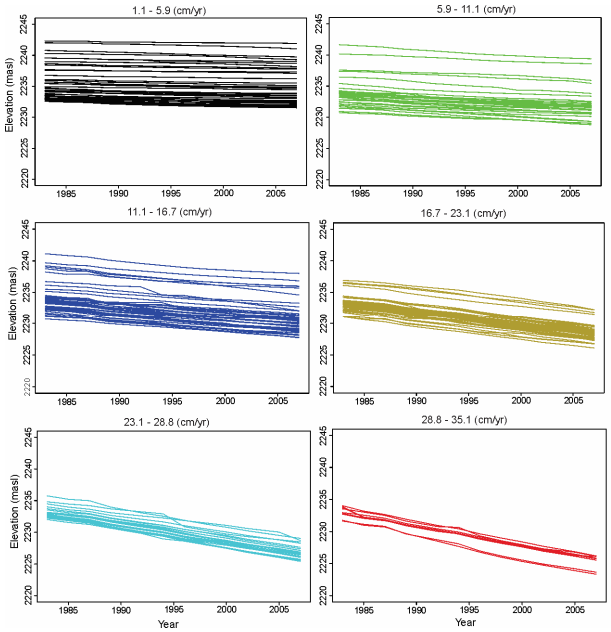

Figure 3. Evolution of ground elevations between 1983 and 2007

Figure 3 gives information about the evolution of ground elevation measurements during 24 years of monitoring within the subsidence rate classes (Figure 2). In this figure, each line represents the readings recorded in each topographic reference in the twelve time points (1983, 1985, 1987, 1989, 1992, 1994, 1996, 1998, 2000, 2002, 2005, 2007). It is essential to underline that only a ground elevation measurement was recorded in each considered year. In addition, this figure provides information on the behavior of subsidence rates within each class and highlights the differences between them. On the other hand, this figure shows that the regional subsidence phenomenon is a non-stationary process as it presents a trend over time.

Subsidence rate contour lines were obtained by performing a kriging interpolation using a 100 × 100 m grid (Figure 4). In this figure red zones correspond to areas where subsidence rates are higher.

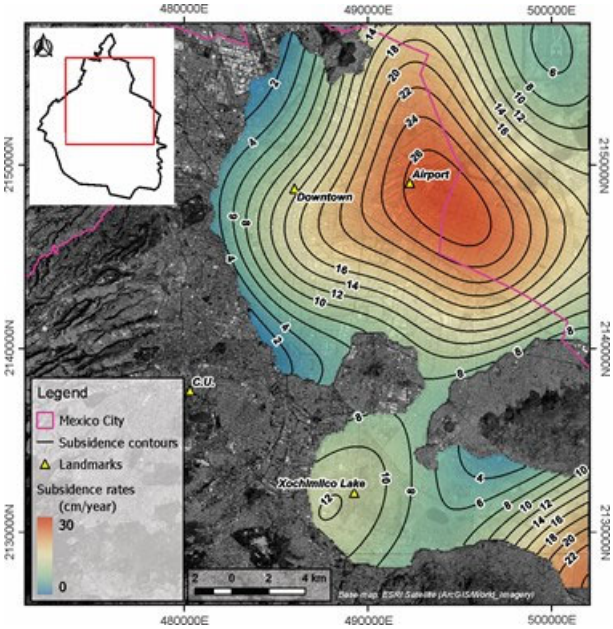

Figure 4. Mean subsidence rate map for the period 1983-2007.

Currently, besides the conventional leveling of surface benchmarks, the use of satellite images has also allowed analyzing the sinking of Mexico City, providing a better spatial resolution and a general overview of the phenomenon. Researchers such as Cabral-Cano et al. (2008, 2011) Osmanoğlu et al. (2011) and Hernández-Espriu et al. (2014) have used this data to study the variations in subsidence rates and land deformation. Overall, the subsidence rate spatial pattern and the location of the maximum rate values in the eastern part of Mexico City, close to the boundaries of the ex-Texcoco Lake, presented in the subsidence rate maps of these studies, agree with the one shown in Figure 4 for the 1983–2007 period.

3.2 *Structural analysis*

Since the regional subsidence phenomenon is not a stationary process as it presents a trend over time, the spatiotemporal variogram $\gamma(s_i, s_j, t_i, t_j)$ was determined from the stochastic residual function ϵ of the process as follows (Snepvangers et al. 2003):

$$\gamma(s_i, s_j, t_i, t_j) = \frac{1}{2} E\left[\left(\epsilon(s_i, t_i) - \epsilon(s_j, t_j)\right)^2\right] \quad (5)$$

Under the assumptions of stationarity, an estimate of the spatiotemporal variogram can be obtained by calculating the empirical semivariogram $\hat{\gamma}(h_S, h_T)$ from the observations as it is shown in Equation (6) (Snepvangers et al. 2003).

$$\hat{\gamma}(h_S, h_T) = \frac{1}{2N(h_S, h_T)} \sum_{i=1}^{N(h_S, h_T)} \left[\left(\epsilon(s, t) - \epsilon(s + h_S, t + h_T)\right)^2\right] \quad (6)$$

where, h_S and h_T are the distances in space S and time T, respectively, and $N(h_S, h_T)$ corresponds to the number of pairs.

The residual function technique separates the non-stationary component of the phenomenon (the trend or mean), $\mu\,(s,t)$, of the stationary residual component, $\epsilon(s,t)$. Then this residual dataset will have a constant mean and its variogram will depend only on the spatial lag (h_S) and temporal lag (h_T).

A 2D-plot and a 3D wireplot of the empirical spatiotemporal semivariogram are shown in Figure 5. This semivariogram was determined based on ground-level readings from each considered benchmark. In this figure, semivariance values vary between 0 (purple color) and 9 (yellow color), approximately. In general, low semivariance values are observed at a short distance because points that are closer together are more alike. As pairs of locations become farther apart, they are more dissimilar and semivariance values increase.

It is essential to notice that in this case, it was assumed that any two temporally consecutive observations have the same temporal distance.

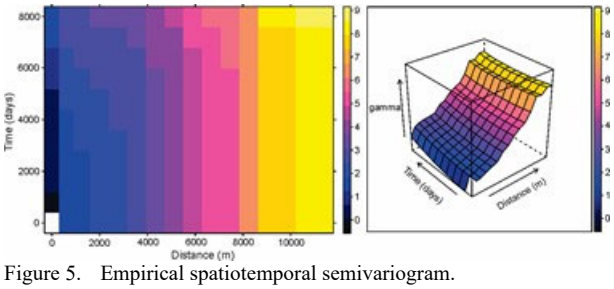

Figure 5. Empirical spatiotemporal semivariogram.

Finally, the pooled variogram $\gamma(\tilde{h})$ where the spatial correlation of the residual ϵ is considered constant over time was also determined as follows:

$$\gamma(\tilde{h}) = \frac{1}{2\sum_{i=1}^{12} N\,(h_S)} \sum_{i=1}^{12} \sum_{j=1}^{N(h_S)} \left[\left(\epsilon(s,t) - \epsilon(s+h_S,t) \right)^2 \right] \tag{7}$$

where, i=1, …,12 correspond to the monitoring years and $N(h_S)$ are the number of pairs of points that are separated by a distance $\tilde{h}$ in year t. The solid line in Figure 6 is the fitted model for the pooled variogram: a Gaussian model with a nugget of 1.25, a range of 5725.92 m, and a sill of 5.77.

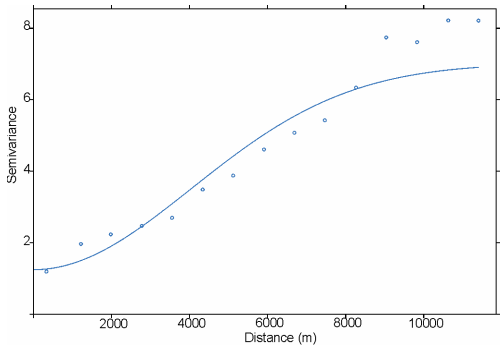

Figure 6. Pooled variogram.

3.3 *Fitting variogram models*

The parameters of the functions fitted to the marginals and pooled data semivariograms were considered as initial values to fit the separable, product-sum, and sum-metric variogram models using the R gstat package (Equation (1), (2), and (4)).

Table 1. Root mean square deviation.

Model	RMSD
Separable	0.0645
Product-sum	0.0663
Sum-metric	0.0819

Table 1 shows that the *separable* model characterizes the behavior of the data adequately by having the lowest value of the RMSD. Gaussian functions were fitted to the marginal experimental semivariograms obtained from the *separable* model. Figure 7 shows that this model adequately represents the variation in space and time of the phenomenon.

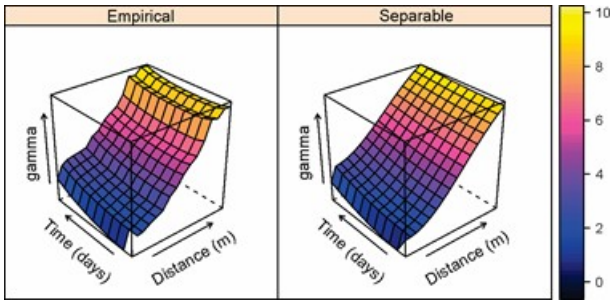

Figure 7. Wireframe plot of empirical spatiotemporal semi-variogram between the period 1983–2007 and fitted space–time variogram.

After fitting a theoretical model to the empirical semivariogram, predictions of the phenomenon in space and time are made by kriging.

3.4 *Predictions*

To estimate the evolution of the regional subsidence phenomenon in Mexico City, a standard kriging was performed up to the year 2030, considering the benchmark locations as estimation points (Figure 8).

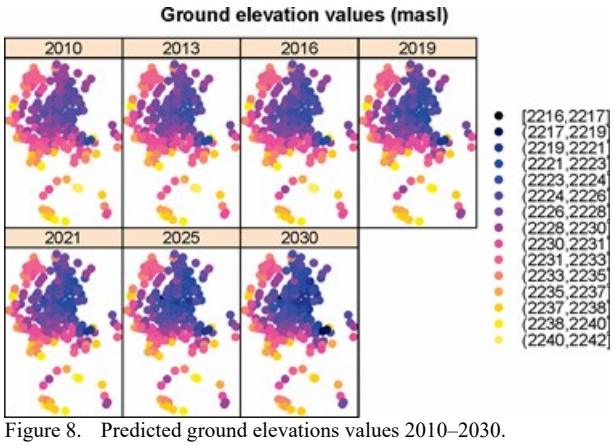

Figure 8. Predicted ground elevations values 2010–2030.

To obtain subsidence rate contour lines, a standard kriging interpolation was performed on a 100 m × 100 m grid, considering a Gaussian variogram model with nugget 10, sill 60, and range 6000 m. Figure 9 shows a mean subsidence rate map between 2007 and 2030 where red zones correspond to areas where subsidence rates are higher, and the blue ones, where they are lower.

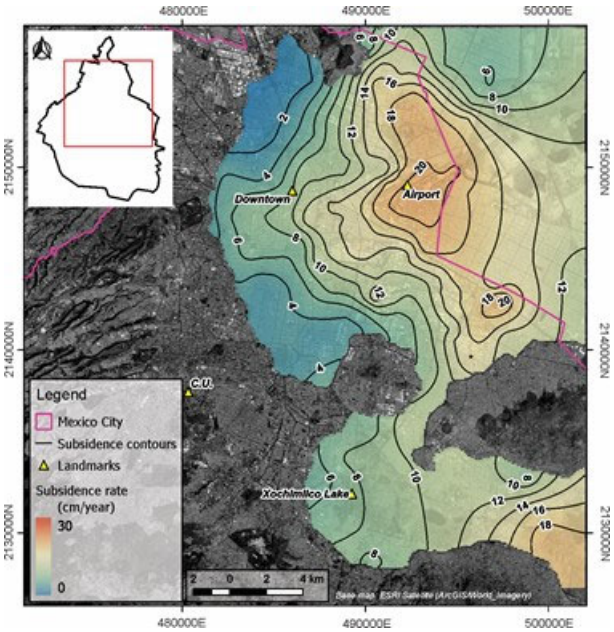

Figure 9. Mean subsidence rate map in the period 2007–2030.

Comparing the subsidence rates determined between 1983 and 2007 with the ones predicted from the geostatistical model between 2007 and 2030, it can be observed that they slow by approximately 30% and that is in agreement with results obtained by other authors (Avilés and Pérez- Rocha, 2010), the most significant changes in subsidence rate values are associated with the thickness of the clay deposits. However, it is essential to note that this model simplifies a complex process involving the rate of groundwater extraction, volumetric compressibility, and hydrogeological factors, among others, which are not considered. This model represents the spatial and temporal correlation of ground benchmark readings located in the lacustrine zone of Mexico City over 24 years of monitoring.

3.5 *Validation of the predictions*

The validation process involved comparing direct measurements from 2016 and 2021 benchmarks with the corresponding ground elevations obtained from the model for the same years. This process was made to verify that the predicted values from the space-time model physically represent the behavior of regional subsidence in Mexico City.

Equation (8) was used to determine the errors, ε, between the registered ground elevations and those predicted by the space-time model.

$$\varepsilon = measured\ value - predicted\ value \quad (8)$$

Table 2. Error in meters for 2016.

Error	Benchmarks
0.00 – 0.29	176
0.39 – 1.00	27
1.00 – 2.24	2
2.24 – 5.06	1

Table 3. Error in meters for 2021.

Error	Benchmarks
0.00 – 0.39	174
0.39 – 1.22	29
1.22 – 3.66	2
3.66 – 7.20	1

Table 2 and Table 3 show the error in meters obtained in each benchmark for 2016 and 2021, respectively. Here it can be observed that they have little variability ($\sigma^2 = 0.21$ and 0.45), and that, in general, at 84% of the sites the difference between the measured and predicted values is less than 0.4 m. This implies that, in general, accurate ground elevation values and subsidence rates can be obtained from the proposed space-time model during the period 2010-2030 for the lacustrine zone of Mexico City.

4 CONCLUSIONS

As there is no specific theoretical or empirical method to analyze the regional subsidence in the lacustrine area of Mexico City, a geostatistical method was developed to estimate the spatial and temporal evolution of this phenomenon between 2010 and 2030 by considering topographic reference information recorded between 1983 and 2007. However, it is essential to notice that the model presented in this paper simplifies a complex phenomenon where geological, hydrogeological, and geotechnical factors are involved, which were not included. Furthermore, limited spatial information was considered because a complete grid layout was used, as a first approximation, to determine the spatial and temporal correlation of the phenomenon in the area of study. This grid represents a combination of spatial and temporal attributes, where every spatial feature has a time observation point (i.e., benchmarks with missing level readings in any monitored year were not considered). An improvement of the model could be made by considering a sparse grid layout to include more spatial information.

Based on the RMSD value, the separable model was the one that best represented the spatial and temporal correlation of the observations of the phenomenon in the area of study, so it was considered to perform a spatio-temporal Kriging to predict the ground level values during the period 2010-2030. It is essential to notice that this model assumes that the temporal behavior of the process is the same for all spatial points, i.e., this model does not allow changes in the spatial pattern over time.

Although geotechnical factors such as the variability of soil properties, stress conditions, and stress histories in clay masses were not included in the geostatistical model, the most significant changes in subsidence values are associated with the thickness of the clay deposits in the lacustrine zone of Mexico City.

Predictions were made until 2030 because the results obtained at the sites where the benchmarks are located showed that the phenomenon would follow constant behavior, implying that this consolidation process will eventually stop, which is incorrect. As the prediction time increases, the uncertainty of the results will also increase because of the lack of recent level information that could be included in the model. Although this geostatistical model has its limitations, it provides valuable information that could help the respective authorities to make better decisions about further urban development and to identify the existing infrastructure that could suffer significant damage because of differential settlement.

The validation process involved comparing direct measurements from 2016 and 2021 with the corresponding ground elevations obtained from the model for the same years. It was observed that in 84% locations points, differences were less than 0.40 m and they had little variability.

5 REFERENCES

Arroyo, D., Ordaz, M., Ovando-Shelley, E., Guasch, J.C., Lermo, J., Pérez, C., Alcántara, L., and Ramírez-Centeno, M.S. 2013.

Evaluation of the change in dominant periods in the lake-bed zone of Mexico City produced by ground subsidence through the use of site amplification factors. *Soil Dynamics and Earthquake Engineering* 44, 54-66.

Avilés, J., and Pérez-Rocha, L. 2010. Regional subsidence of Mexico City and its effects on seismic response. *Soil Dynamics Earthquake Engineering* 30 (10), 981-989.

Bilonick, R.A. 1988. Monthly hydrogen ion deposition maps for the northeastern U.S. from, July 1982 to September 1984. *Atmospheric Environment* 22(9),1909–1924.

De Cesare, L., Myers, D., and Posa D. 2001. Estimating and modeling space- time correlation structures. *Statistics Probability Letters* 51(1), 9–14.

Cabral-Cano, E., Dixon, T.H., Miralles-Wilhelm, F., Díaz-Molina, O., Sánchez-Zamora, O., and Carande, R.E. 2008. Space geodetic imaging of rapid land subsidence in Mexico City. *Bulletin Geological Society of America* 120,1556–1566.

Cabral-Cano, E., Díaz-Molina, O., and Delgado-Granados, H. 2011. Subsidencia y sus mapas de peligro: un ejemplo en el área nororiental de la Zona Metropolitana de la Ciudad de México. *Boletín De La Sociedad Geológica Mexicana* 63,53–60.

Cressie, N.A. 1993. Statistics for spatial data. Wiley, New York.

De Iaco, S., Myers, D., and Posa D. 2001. Space-time analysis using a general product-sum model. *Statistics Probability Letters* 52(1), 21-28.

De Iaco, S., Myers, D., and Posa, D. 2011. One strict positive definiteness of product and product-sum covariance models. *Journal of Statistical Planning and Inference* 141,1132-1140.

Gräler, B., Pebesma, E., Heuvelink, G. 2016. Spatio-Temporal Interpolation using gstat. *R Journal* 8(1),204–2018.

Gringarten, E., Deutsch, C. 2001. Teacher's aide: Variogram interpretation and modeling. *Mathematical Geology* 33 (4), 507-534.

Hernández-Espriú, A., Reyna-Gutiérrez, J.A., Sánchez-León, E., Cabral-Cano, E., Carrera-Hernández, J., Martínez-Santos, P., Macías-Medrano, S., Falorni, G., and Colombo, D. 2014. The DRASTIC-Sg Model: a new extension to the standard DRASTIC approach for mapping groundwater vulnerability in urban aquifers subject to differential land subsidence with application to Mexico City. *Hydrogeology Journal* 22, 1469-1485.

INEGI. 2020. Instituto Nacional de Estadística y Geografía [Online] Available at: https://www.inegi.org.mx/ [Accessed July 2025].

Jenks, G.F, and Caspall, F.C. 1971. Error on choroplethic maps: definition, measurement, reduction. *Annals of Association of American Geographers* 61,217–244.

Kyriakidis, P.C., and Journel A.G. 1999. Geostatistical space-time models: A review. *Mathematical Geology* 31(6), 651-684.

Osmanoğlu, B., Dixon, T.H., Wdowinski, S., Cabral-Cano, E., and Jiang, Y. 2011. Mexico City subsidence observed with persistent scatterer InSAR. *International Journal of Applied Earth Observation and Geoinformation* 13,1–12.

Ossa, A., Botero, E., Madrigal, M.C., Ovando, E., Mendoza, M., and López-Acosta, N.P. 2019. Performance of a pavement foundation system based on the partial compensation of masses method. *Soils and Foundations* 59, 351-366.

Ovando, E., Romo, M.P., Contreras, N., and Giralt, A. 2003. Effects on soil properties of future settlements in downtown Mexico City due to ground water extraction. *Geofísica Internacional* 42(2), 185-204.

Ovando, E., Ossa, A., and Santoyo, E. 2013. Effects of regional subsidence and earthquakes on architectural monuments in Mexico City. *Boletín de la Sociedad Geológica Mexicana* 65 (1), 157-167.

Pebesma, E. 2012. Spacetime: Spatio-Temporal Data in R. *Journal of Statistical Software* 51(7), 1-30.

R Core Team.1993. R: A Language and Environment for Statistical Computing. R Foundation for Statistical Computing, Vienna.

RStudio Team. 2015. RStudio: Integrated Development for R. RStudio Inc, Boston.

Shapiro, N.M., Singh, S.K., Almora, D., and Ayala, M. 2001. Evidence of the dominance of higher-mode surface waves in the lake-bed of the Valley of Mexico. *Geophysical Journal International* 147, 517-527.

Snepvangers, J., Heuvelink, G., and Huisman J. 2003. Soil water content interpolation using spatio—temporal kriging with external drift. *Geoderma* 112, 253–271.

SIMOH. 2015. Sistema de Monitoreo de la Piezometría y de los Hundimientos del Valle de México por Extracción de Agua Subterránea. Informe Final elaborado para la Comisión Nacional del Agua (CONAGUA). Convenio: CGPEAYS-UNAM-04/2013. Instituto de Ingeniería de la UNAM.